Annals of Biomedical Engineering, Vol. 25, pp. 678–689, 1997
Printed in the USA.

0090–6964/97 $10.50 + .00

A Small Angle Light Scattering Device for Planar Connective Tissue Microstructural Analysis

MICHAEL S. SACKS, DAVID B. SMITH, and ERIK D. HIESTER

Tissue Mechanics Laboratory, Department of Biomedical Engineering, University of Miami, Coral Gables, FL

Abstract—The planar fibrous connective tissues of the body are composed of a dense extracellular network of collagen and elastin fibers embedded in a ground matrix, and thus can be thought of as biocomposites. Thus, the quantification of fiber architecture is an important step in developing an understanding of the mechanics of planar tissues in health and disease. We have used small angle light scattering (SALS) to map the gross fiber orientation of several soft membrane connective tissues. However, the device and analysis methods used in these studies required extensive manual intervention and were unsuitable for large-scale fiber architectural mapping studies. We have developed an improved SALS device that allows for rapid data acquisition, automated high spatial resolution specimen positioning, and new analysis methods suitable for large-scale mapping studies. Extensive validation experiments revealed that the SALS device can accurately measure fiber orientation for up to a tissue thickness of at least 500 μm to an angular resolution of ~1° and a spatial resolution of ±254 μm. To demonstrate the new device's capabilities, structural measurements from porcine aortic valve leaflets are presented. Results indicate that the new SALS device provides an accurate method for rapid quantification of the gross fiber structure of planar connective tissues.

Keywords—Collagen, Fiber architecture, Lasers, Light scattering, Optical methods, Heart valves.

INTRODUCTION

The planar fibrous connective tissues of the body are generally composed of a dense extracellular network of collagen and elastin fibers, embedded in a ground matrix consisting of proteoglycans and water (8). It is well known that collagen fibers can withstand high tensile force, but appear to have low torsional and flexural stiffness (10). Thus, directions in which the fibers are oriented can be identified with the directions in which the tissue is ableto withstand the greatest tensile stresses. Gross fiber orientation thus leads to an understanding and predictability of the mechanical properties of the tissue. For example, the structure of the aortic heart valve is uniquely suited for efficient transmission of mechanical stresses with the minimal use of material. Although available microscopic techniques can provide quantitative information on fiber structure (15), this information is by definition highly localized, making it difficult to quantify larger scale fiber structural features. Thus we need a rapid method to map the complete gross fiber structure of planar tissues.

Several methods have been previously used for the analysis of the fiber architecture in soft tissues (15). Image processing techniques, which use either optical (35) or scanning electron microscopic images (4,9,19), have been used to provide highly localized information on the size and orientation of fibers. However, these are destructive approaches requiring time-consuming tissue preparations and are thus not suitable to large-scale mapping studies. Small angle X-ray scattering techniques have been used to analyze the collagen molecular architecture (15,16,25,31). Scattering patterns are recorded on film, which require long exposure times, and the technique suffers from similar mapping limitations of the electron microscopy methods.

In the technique of small angle light scattering (SALS), laser light is passed through a tissue specimen, and the spatial intensity distribution of the resulting scattered light represents the sum of all structural information within the light beam envelope. HeNe is used because its wavelength (λ = 632.8 nm) is within an order of magnitude of the diameter of the collagen and elastin fibers, SALS has been used to quantify the fibrous structure of both polymers (2,23,26,33,34) and collagen films (5,22). Kronick and Buechler (17) found close agreement between the fiber orientation measurements made by SALS and X-ray diffraction, indicating that SALS was an inexpensive alternative to X-ray diffraction for

Acknowledgment—The support of the A. W. Ford Foundation and the American Heart Association, Florida Affiliate, is gratefully acknowledged. M. S. Sacks would like to thank Dr. Paul L. Kronick of the United States Department of Agriculture–Eastern Regional Center for introducing him to the use of SALS as a method for connective tissue structural analysis. The authors would also like to acknowledge Kristen L. Billiar and G. Regunath for their assistance in the SALS device design and fabrication.

Address correspondence to Dr. Michael S. Sacks, Department of Biomedical Engineering, P.O. Box 248294, University of Miami, Coral Gables, FL 33124-0621, U.S.A.

(Received 9Apr96, Revised 8Nov96, Revised 4Dec96, Accepted 5Dec96)

quantitative measurements of soft tissue fibrous networks.

Sacks and Chuong (28) expanded the use of SALS to the study the diaphragmatic central tendon (DCT), using similar methods developed in the analysis of calf dermis structural defects (18). By performing SALS tests throughout the tissue, a map of the fiber architecture of the DCT was generated. Structural data were consistent with the direction and degree of mechanical anisotropy (6). We have also used SALS to study the relation between fiber architecture and biaxial mechanical anisotropy in bovine pericardium (29), suggesting that SALS is a successful method for mapping the gross fiber structure of tissues used in heart valve bioprostheses.

The previous SALS devices used rotating photodiode arrays to digitize the scattered light intensity, as well as requiring manual positioning of the specimen (27). Furthermore, analysis of the SALS data was performed using nonlinear curve-fitting methods that required the user to generate initial parameter estimates for each test location (28). The methods of data acquisition and analyses are clearly unsuitable for practical applications of large fiber structure mapping. With these considerations in mind, we have developed an improved SALS device that uses high-resolution automated specimen positioning and data acquisition for rapid scanning of large areas of tissue. New, fully automated analysis methods were also developed that eliminated the need for user intervention. The results from extensive accuracy, sensitivity, and resolution studies are presented, as well as structural measurements from bovine pericardium and porcine aortic valve leaflets to demonstrate the new device's mapping capabilities.

METHODS

Hardware Description

The SALS device consists of an unpolarized 4 mW HeNe laser (λ = 632. 8 nm; Uniphase, Manteca, CA, USA), spatial filter-beam expander, sample positioner, projection screen, and a CCD NTSC-compatible auto-iris videocamera (Model SSC-M350, Sony, Inc., Tokyo, Japan) equipped with a telecentric lens to minimize image distortion (Edmund Scientific, Barrington, NJ, USA), all mounted on a rigid optical platform (Fig. 1). Since the laser has a Gaussian intensity profile, we used the common definition of the beam diameter as that diameter of the laser beam core that contains all but $1/e^2$ (*i.e.*, 13.5%) of the total radiant beam power (20). Thus, all beam diameters reported in this study contain 86.5% of the total beam intensity. As the laser light passes through the tissue, it is scattered by the fibrous structures, and the resultant scattering pattern is cast onto the projection screen (Fig. 1). The video image of the scattered light is digitized to a resolution of 640 × 480 8-bit pixels using a Data Translation image grabber board (Model 3851; Marlboro, MA, USA) mounted in the 486/33 MHz PC (Fig. 1). The image grabber board has sufficient video memory to allow for image analysis while the subsequent image is being acquired.

The sample positioner allows for two axes of movement in a plane perpendicular to the optic axis (Fig. 1). Both axes use a precision linear travel system using 16 threads/inch of lead screws with anti-backlash nuts. Positioning of each axis is accomplished by rotating the lead screws using two PC-controlled stepper motors (Arrick Robotics, Hurst, TX, USA) with 400 steps/rev resolution,

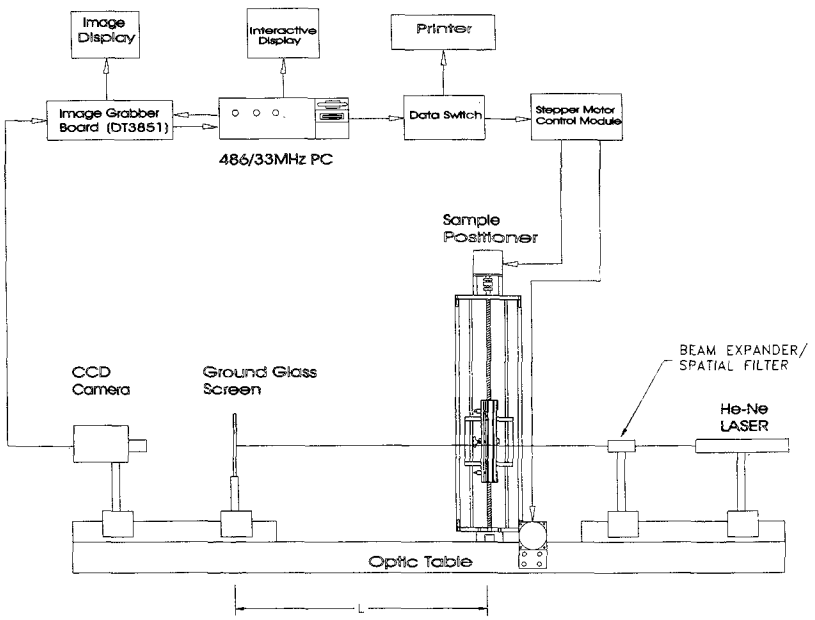

FIGURE 1. A schematic of the SALS device, which consists of an unpolarized 4 mW HeNe laser, spatial filter-beam expander, sample positioner, projection screen, and a CCD videocamera. The sample positioner allows for two axes of movement in a plane perpendicular to the optic axis. All motion control, video processing, and data analysis are performed by custom C++ programs that can scan one test location in ~1 sec.

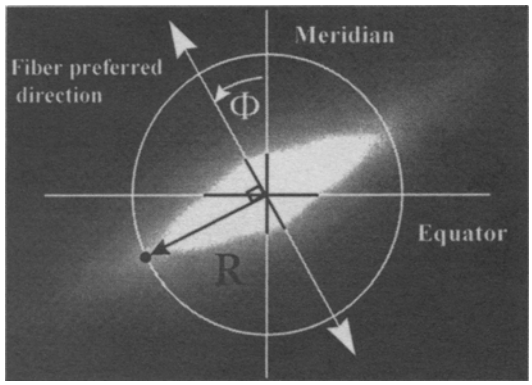

(a)

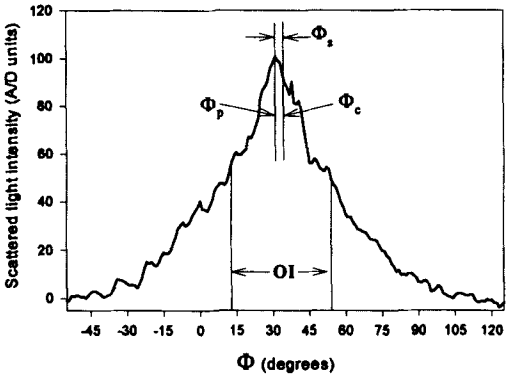

(b)

FIGURE 2. (a) A digitized image of the scattered light intensity from a porcine aortic valve. The *I*(Φ) *versus* Φ data is extracted from the SALS image along a circle of radius *R* centered on the optic axis (dot on circle), corresponding to a scattering angle $\theta = \tan^{-1}(R/L)$, where *L* is the distance from the specimen to the projection screen (Fig. 1). (b) The extracted *I*(Φ) versus Φ data, showing the locations of Φ_p, Φ_c, and the definition of the distribution skew, $\Phi_s = \Phi_p - \Phi_c$. Because light is scattered perpendicular to the fiber axes, all *I*(Φ) measurements are automatically shifted by 90°, so that *I*(Φ) represents the true fiber orientation.

resulting in a net movement resolution of 4 μm/step and a total travel range of 25 cm along each axis. All motion control, video processing, and data analysis are performed by custom-written C++ programs (Turbo C++ 3.0, Borland; Scotts Valley, CA, USA). This system allows for video acquisition, initial data analysis (see below), storage of the analyzed data to the hard disk, and movement to the next test location, all in ~1 sec.

Analysis of the Light Scattering Pattern

Assuming no optical interactions, a fibrous network optically behaves like a two-dimensional assembly of single slits. In the case of dense fibrous tissues, the effective slit width is an average of the fiber diameters and the spaces between the fibers (see the Appendix). According to single-slit diffraction theory, light is scattered in a direction perpendicular to the fiber axis (13), although there will be no observable minima due to the distribution of "slit" widths (*i.e.*, fiber diameter and interfiber spaces) in the tissue. Each fiber, having an angular orientation Φ, will thus contribute its scattered light intensity at an angular orientation of Φ + 90°. As long as the fiber diameter and interfiber spacing distribution are independent of Φ, the angular distribution of scattered light at a constant θ represents the angular distribution of fibers about the optic axis within the light beam envelope (Fig. 2).

To extract the angular fiber orientation information, scattered light intensity values were taken from the digitized SALS image at 1° increments through the angle Φ about a circle corresponding to a constant θ centered on the optical axis (Fig. 2a). The extracted intensity distribution, I(Φ), is taken as the average detected intensity using a 3 × 3 pixel grid centered on the current pixel location. Because light is scattered perpendicular to the fiber axes, all I(Φ) values are actually acquired at Φ + 90°, so that I(Φ) represents the true fiber orientation (Fig. 2a).

Because the light scattering pattern is symmetric about the preferred fiber direction, the I(Φ) versus Φ distribution is repeated twice over the full 360° range (Fig. 2). The two intensity minima will demarcate where the axis of symmetry occurs in the scattering pattern, with the data from either symmetric segment usable for analysis. From each

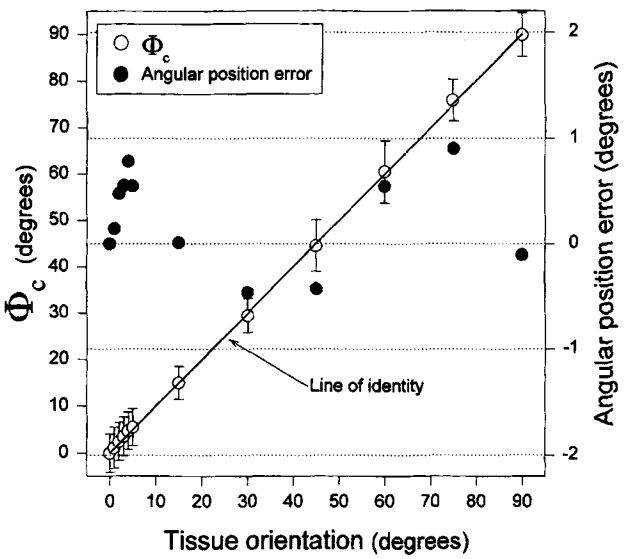

FIGURE 3. Mean Φ_c and angular position error *versus* specimen orientation Φ for a 500 μm bovine tendon section for $0° \le \Phi \le 90°$. For all orientations, there was close agreement between measured and actual (line of identity) Φ values, along with angular position errors all below 1°. These results indicate a ~1° angular resolution in Φ_c.

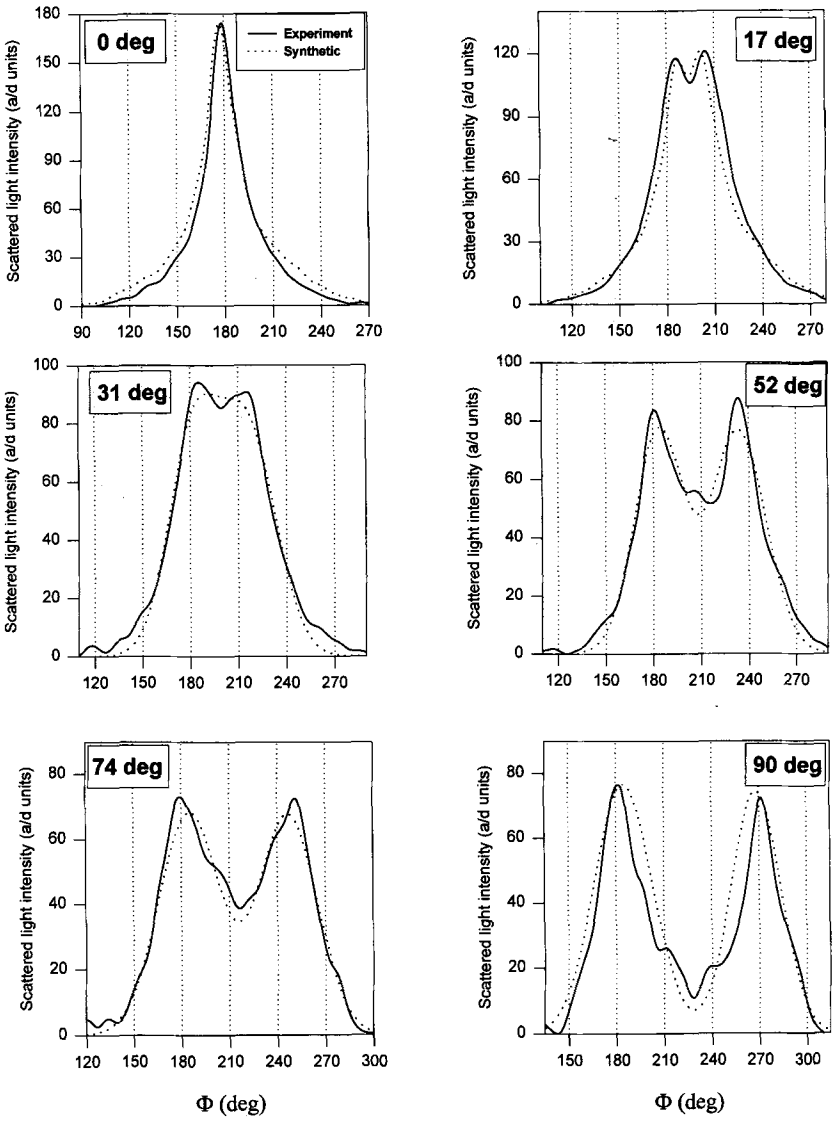

FIGURE 4. I(Φ) *versus* Φ data for two overlapping 200 μm bovine tendon sections rotated 0°, 17°, 31°, 52°, 74°, and 90°, with respect to their preferred directions, showing both the experimentally measured and synthetically generated data. The second specimen's fiber orientation distribution can be seen to become increasingly distinct as the angle between the two specimens increases. Good agreement can be see between the experimentally measured and synthetically generated data for all values of Φ.

symmetric 180° segment, the preferred fiber directions, degree of symmetry of the fiber distribution about the preferred direction, and the degree of fiber orientation can be determined (17,28). First, we define the preferred direction as the distribution centroid (Φ_c):

$$\Phi_c = \frac{\sum_{\Phi=\Phi_{min}}^{\Phi_{min}+180^\circ} \left[(\Phi - \Phi_{min}) \frac{I(\Phi) + I(\Phi - 1)}{2} \right]}{\sum_{\Phi=\Phi}^{\Phi_{min}+180^\circ} \left[\frac{I(\Phi) + I(\Phi - 1)}{2} \right]} \quad (1)$$

where the summations are computed directly from a 180° segment (Φ_{min} to $\Phi_{min} + 180°$) of the SALS data using increments of 1° (we arbitrarily choose the segment closest to 0°). Φ_c represents the overall preferred direction of the fiber network and is computed without the need of any distribution model, such as the Gaussian as used in Ref. 28. If the distribution is symmetrical about the Φ_c, the intensity peak Φ_p will coincide with Φ_c (Fig. 2b). Deviation from the condition of symmetry is defined as the distribution skew, $\Phi_s = \Phi_p - \Phi_c$ (Fig. 2b). Note that large values of Φ_s will generally indicate that the fiber angular distribution cannot be considered as a single population, implying the existence of multiple layers of fibers with substantially different orientations.

The width of the I(Φ) *versus* Φ distribution is indicative of the degree of fiber orientation: highly oriented fiber networks result in a very narrow peak, while less well-oriented fibers yield a broader peak. We have previously used the $\langle \cos^2\Phi \rangle$ to compute the degree of orientation normalized to a percentile scale (28). However, the $\langle \cos^2\Phi \rangle$ has no direct physical interpretation and is a nonlinear function of the distribution width. To develop a

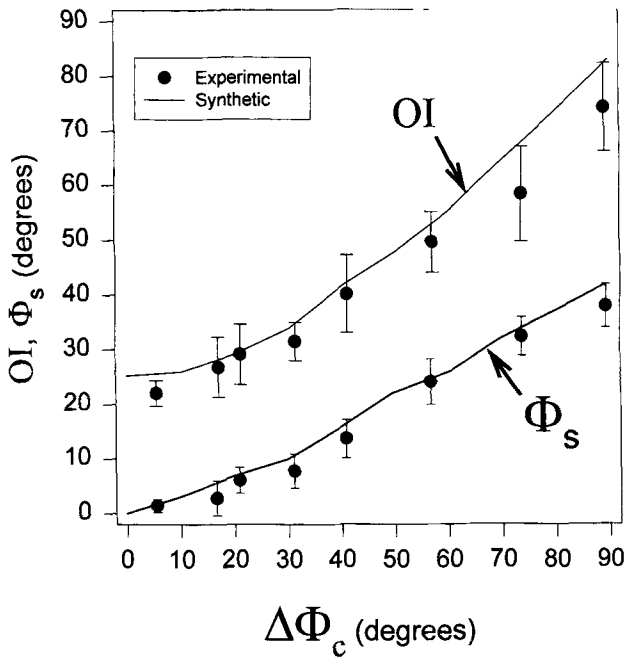

FIGURE 5. Comparison of the measured and "synthetic" SALS analysis for (a) OI and (b) Φ_s using the SALS data of Fig. 4 showing good agreement between experimental and synthetic data. These results indicate that the SALS device can detect multiple populations to ~5° separation in their preferred directions.

physically intuitive orientation index (OI), we used the property of the I(Φ) *versus* Φ distribution that when normalized to a total area of unity, it represents a statistical probability function of fiber orientation. We define a new OI as the angle that contains one-half of the total area under the I(Φ) *versus* Φ distribution, representing 50% of the total number of fibers (Fig. 2b). Thus, highly oriented fiber networks will have low OI values, whereas more randomly oriented networks will have larger values. Note that the OI is computed directly from the I(Φ) *versus* Φ data without the need of any distribution model.

SALS Calibration

Evaluation of the SALS device's capabilities included: (i) assessment of the angular and spatial resolutions, (ii) sensitivity to the presence of multiple fiber populations, (iii) effects of beam diameter, and (iv) effect of tissue thickness. To determine angular resolution, two 10 mm square sections of bovine tendon (chosen for its uniformity in fiber structure, see Ref. 28) 100 and 500 μm thick, were mounted on a rotatable positioning device and tested at angular positions ranging from 0° to 90°. SALS data were acquired over the entire specimen using a 1-mm-spaced rectilinear grid.

When two fiber populations exist, the resultant SALS data will contain two overlapping populations (28). Sensitivity to multiple populations was determined using two 200 μm bovine tendon sections placed partially overlapping each other in the SALS device. One specimen was rotated with respect to the other for values of the difference in preferred directions, $\Delta\Phi_c$, ranging from 0° to 90°. I(Φ) was acquired for each $\Delta\Phi_c$ value from the overlapping area of the sections using a 254-μm-spaced testing rectilinear grid. Because we assumed no optical interaction between fibers, the resultant scattering pattern of the overlapping sections should be the sum of the two individual layers. To test this assumption, we summed the SALS data from the individual bovine tendon sections at the same $\Delta\Phi_c$ values used in the overlapped sections to generate "synthetic" multiple population SALS data. Both the Φ_s and OI were computed from the synthetic datasets and compared with the actual overlapping tissue SALS measurements. The effect of beam diameter on SALS spatial resolution was also determined using the same two sections, which were scanned using a 254 μm rectilinear grid and 100, 350, and 500 μm beam diameters.

As tissue thickness increases, multiple scattering effects caused by light rescattered by succeeding collagen fiber layers also increases, causing potential loss of structural information (7,12). It was previously determined using bovine tendon, a dense collageneous tissue, that thicknesses up to 400 μm do not detectably effect SALS measurements (28). To assess more fully the effects of bioprosthetic heart valve (BHV) tissue thickness, SALS data were acquired from a 19 mm square specimen of bovine pericardium using a 2.5 mm increment grid. Next, the specimen was frozen and sectioned at 25 μm increments using a freezing microtome, with sections mounted on a glass slide. SALS data were acquired for each individual section using the same scanning grid, with care taken to ensure consistent registration of the SALS test locations for all sections. The results of the intact tissue and the individual sections could then be compared with determined differences in the SALS data between the individual sections and the intact, full thickness tissue.

Maps of the Collagen Fiber Architecture

To demonstrate the SALS device's capabilities to provide detailed fiber orientation information, we SALS-tested porcine aortic valve leaflets as follows. Fresh porcine aortic valve leaflets were obtained fresh from a slaughterhouse, and fixed under a constant transvalvular pressure of 0 and 4 mm Hg for 24 hr in buffered 0.625% glutaraldehyde solution. The leaflets were then dissected from the aorta, cleared for maximal tissue transparency using graded glycerol solutions to 100%, and scanned using a 254-μm-spaced rectilinear grid. Vector maps indicating Φ_c were produced, along with color fringe plots of the OI, generated by forming triangular elements whose vertices are the test locations and colors represent the average OI of the three vertex tests.

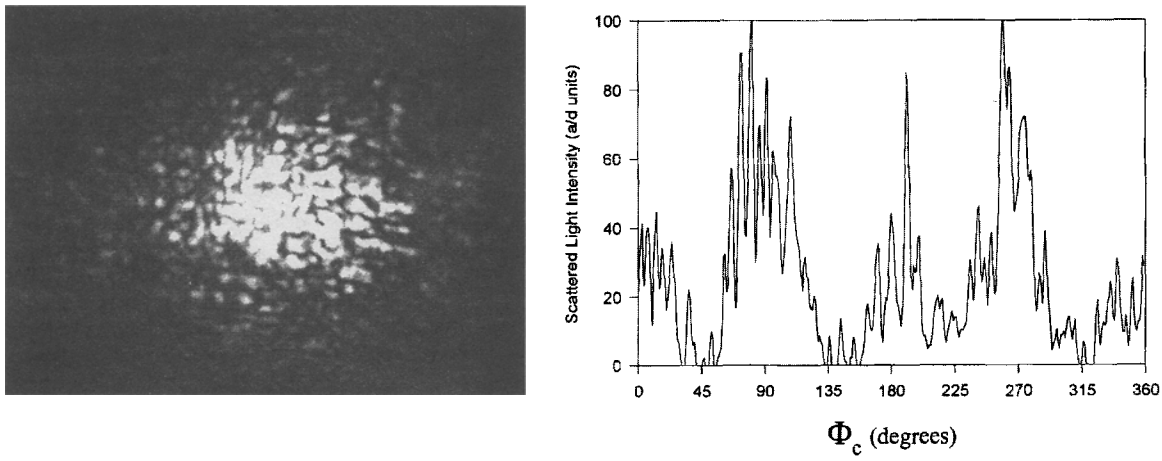

(a)

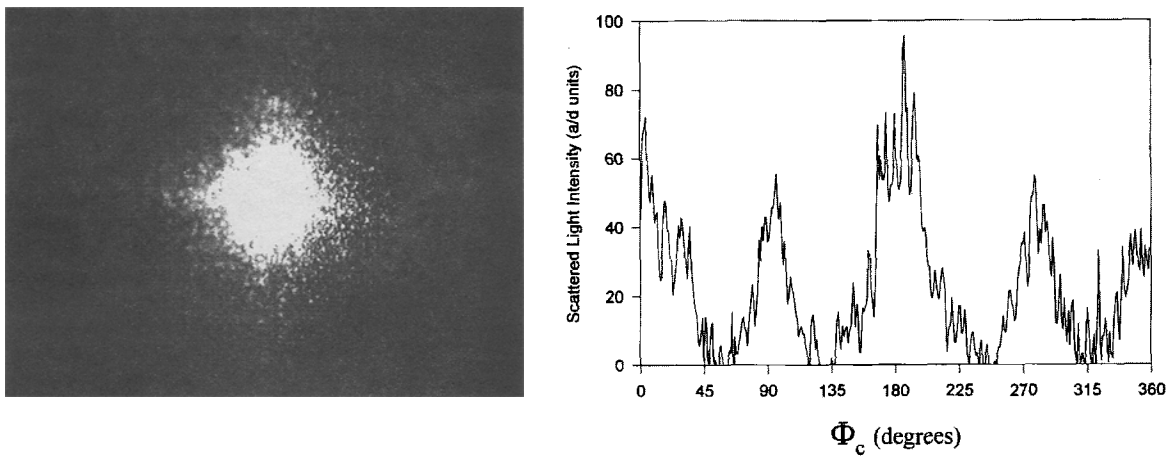

(b)

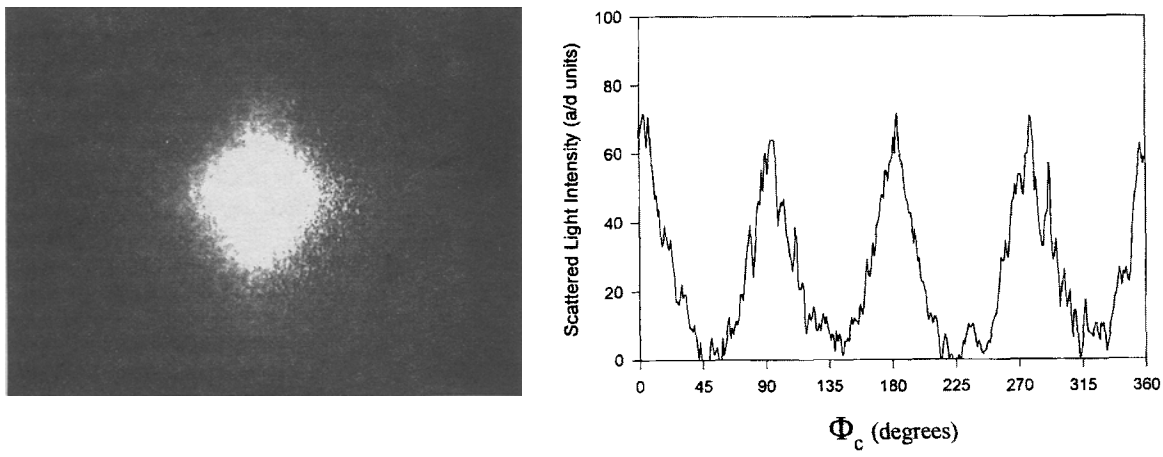

(c)

FIGURE 6. Effects of laser beam diameter on the $I(\Phi)$ *versus* Φ data for (a) 100 μm, (b) 350 μm, and (c) 600 μm $1/e^2$ beam diameters using two overlapping 200 μm bovine tendon sections rotated 90° with respect to their preferred directions. For the 100 and 350 μm beam diameters, speckle interference noticeably degraded the $I(\Phi)$ *versus* Φ data. The best results were obtained with the use of a 600 μm $1/e^2$ beam diameter.

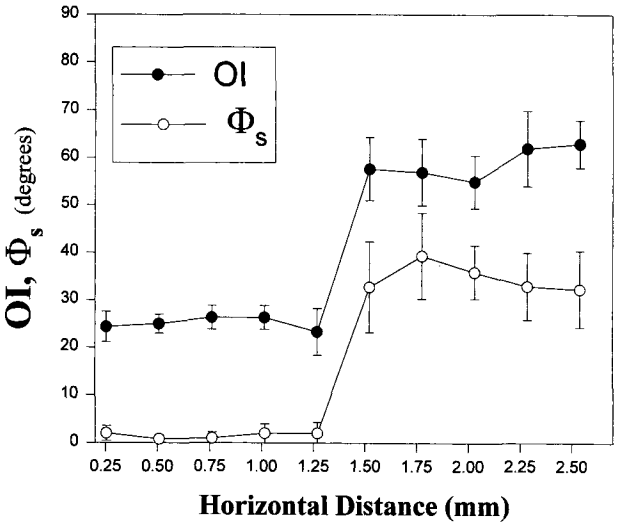

FIGURE 7. OI and Φ *versus* the horizontal distance traversing the boundary between the two overlapping 200 μm bovine tendon sections used in Fig. 6. Both OI and Φ_s will have greater values in the overlapping area, compared with isolated tissue. A sharp, distinct transition occurred at the boundary between the single and overlapping layers of tissue, indicating that the SALS device can distinguish tissue structures to a spatial resolution of 250 μm.

RESULTS

Angular Spatial Resolution and Sensitivity to Multiple Populations

The relationship between true angular position and mean Φ_c was consistently linear, and demonstrated an accuracy of ~1° (Fig. 3). This accuracy was observed for the 100 and 500 μm thicknesses, indicating that the SALS device can accurately distinguish Φ_c up to at least a 500 μm thickness. When multiple populations occur, the gradual separation of the fiber populations becomes clearly visible in the intensity distribution curves as $\Delta\Phi_c$ increases (Fig. 4). There was also close agreement between the experimental and synthetic curves, indicating that the $I(\Phi)$ response is the algebraic sum of the scattered light contributions from the individual bovine tendon sections (Fig. 4). To determine the sensitivity of the SALS parameters (Φ_c, Φ_s, and OI) to multiple populations, the parameters were plotted against the angle between the populations $\Delta\Phi_c$ (Fig. 5). Both Φ_s and OI predictably increased at larger $\Delta\Phi_c$ values, and showed close agreement between the synthetic and experimental data over the complete range of $\Delta\Phi_c$ (Fig. 5). The values for Φ_c computed from the synthetic data were within ±3° of the actual value also over the complete range of $\Delta\Phi_c$. These results indicate that the SALS device can accurately detect the presence of multiple populations when there is at least a ~5° separation in their preferred directions.

Effect of Beam Diameter on SALS Spatial Resolution

As beam diameter is decreased, speckle (*i.e.*, self-interference) becomes more prominent, which appears in the SALS data as random noise that will reduce accuracy (Fig. 6). As the beam diameter increases speckle diminishes, and the scattering pattern becomes more regular. The best data were obtained with a $1/e^2$ beam diameter of 600 μm (Fig. 6), which was used on all tissues in this study.

However, increasing beam diameter will reduce spatial resolution by averaging SALS results over larger tissue areas. To determine the spatial resolution of a 600 μm beam, changes in Φ_s and OI along the horizontal distance transversing the boundary between the two overlapping 200 μm bovine tendon sections were examined (Fig. 7). Both parameters will have lower values (smaller skew/higher degree of orientation) in the single layer area, and a greater value (larger skew/higher degree of orientation) in the overlapping tissue area. A sharp, distinct transition occurred at the boundary between the single and overlapping layers of tissue for both parameters (Fig. 7), indicating that the SALS device can distinguish tissue structures to an effective spatial resolution of ±254 μm with a 600 μm $1/e^2$ beam diameter.

Tissue Thickness Effects Using Bovine Pericardium

SALS results indicated that the overall fiber orientation of the bovine pericardial section changed gradually from the outer (epipericardial) to the inner (visceral) surfaces (Fig. 8a–c). This can be seen to occur at single test location, where the $I(\Phi)$ intensity distribution can be seen to change with thickness (Fig. 8a–c). Because we are assuming no optical interactions between the light scattered from each fiber, the total light scattering pattern should be the algebraic sum of the contributions from each individual fiber layer. To verify this assumption, the SALS data from two locations near the center of each 25 μm section was averaged and compared with the SALS data for sections obtained before sectioning at the same location (Fig. 8d). The close agreement between the averaged and intact SALS data indicates that the SALS pattern is the algebraic sum of the contribution of each layer in the tissue, and that multiple scattering effects due to tissue thickness were negligible.

Effects of Fiber Diameter and Interfiber Spacings

In our treatment of SALS data, we assume that the fiber diameter distribution is *independent* of fiber orientation Φ. As long as this assumption is true, the angular distribution of scattered light intensity accurately represents the angular distribution of fiber orientations. Based on Fraunhofer diffraction theory (see the Appendix), larger fibers tend to scatter light closer to the beam axis and smaller fibers

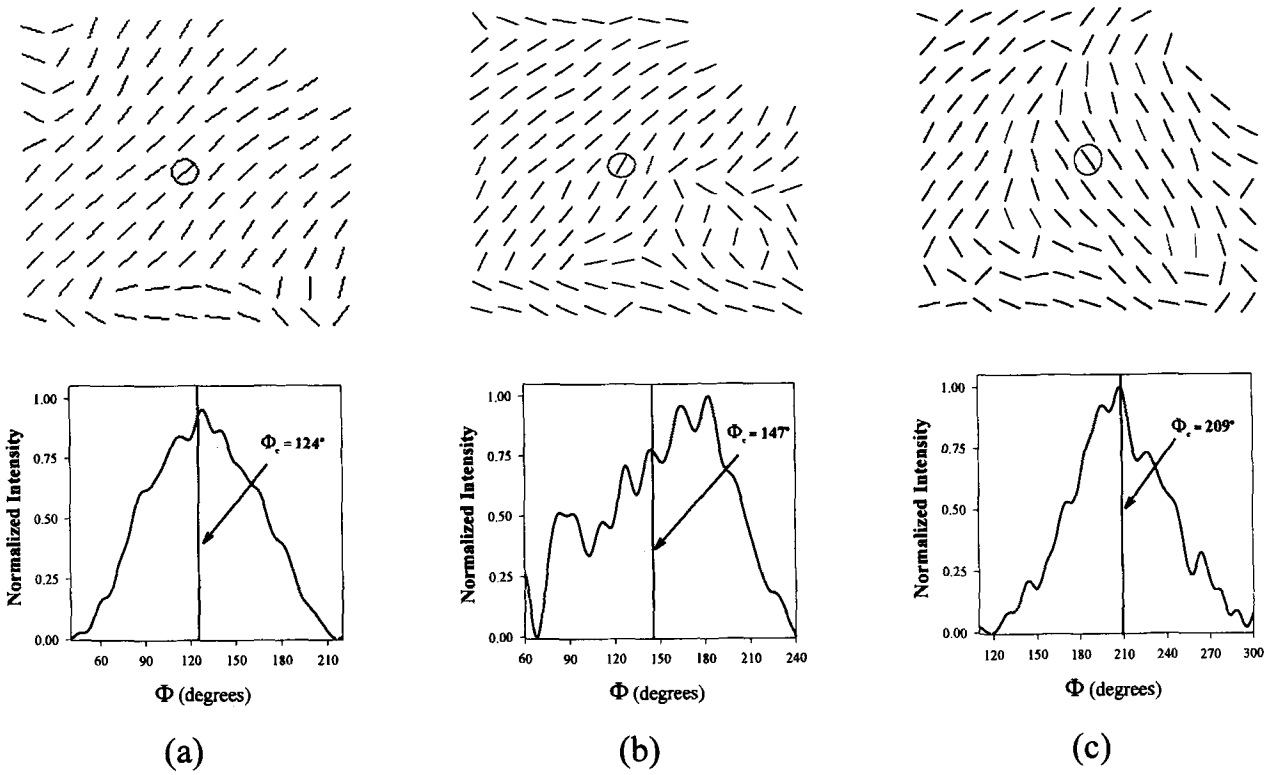

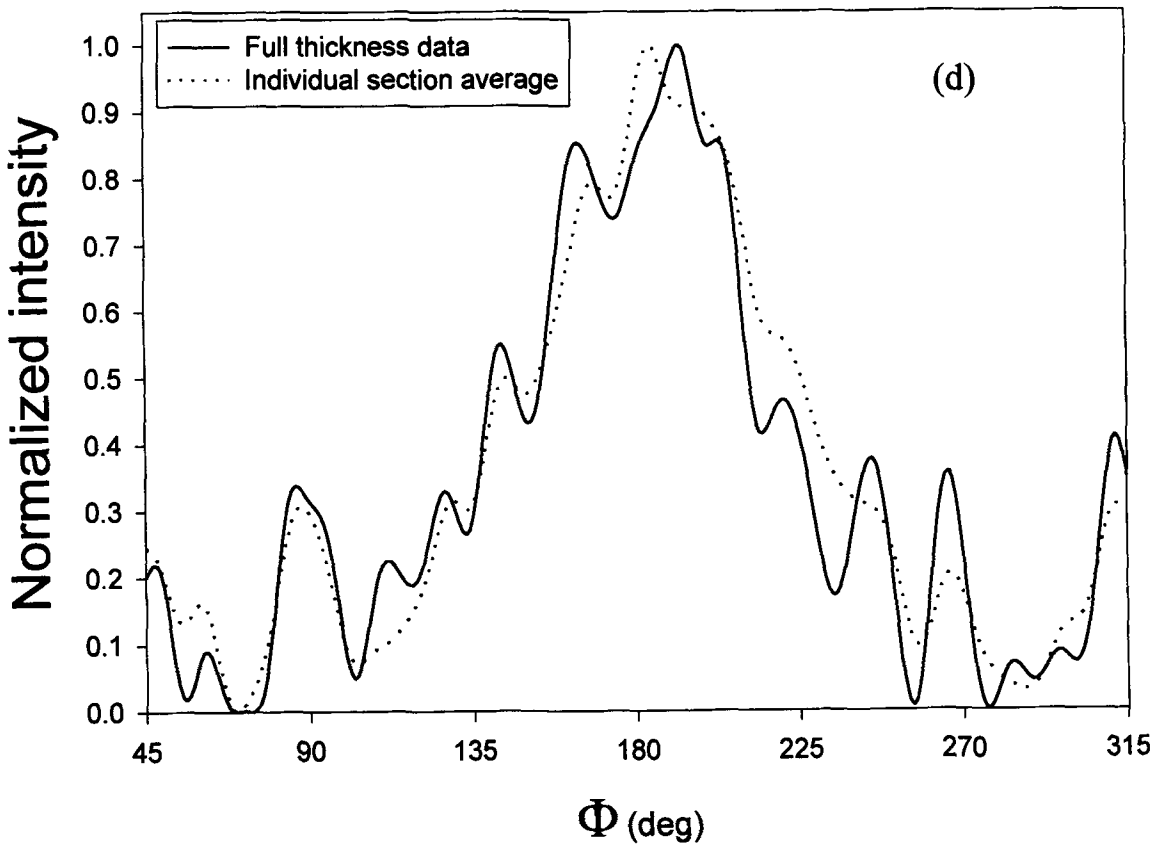

FIGURE 8. Fiber-preferred direction vector plots of sequential 25 μm sections taken from a single bovine pericardium specimen at depths of (a) epipericardial side, (b) 225 μm, and (c) 375 μm (visceral side). I(Φ) *versus* Φ data from each location indicated by the circle is shown in the plots below each vector plot. (d) Averaged normalized I(Φ) versus Φ data from each 25 μm bovine pericardium section shown along with the data from the intact specimen for the location indicated by the circle. The close agreement between the averaged and intact SALS data indicates that the SALS pattern is the algebraic sum of the contribution of each layer in the tissue.

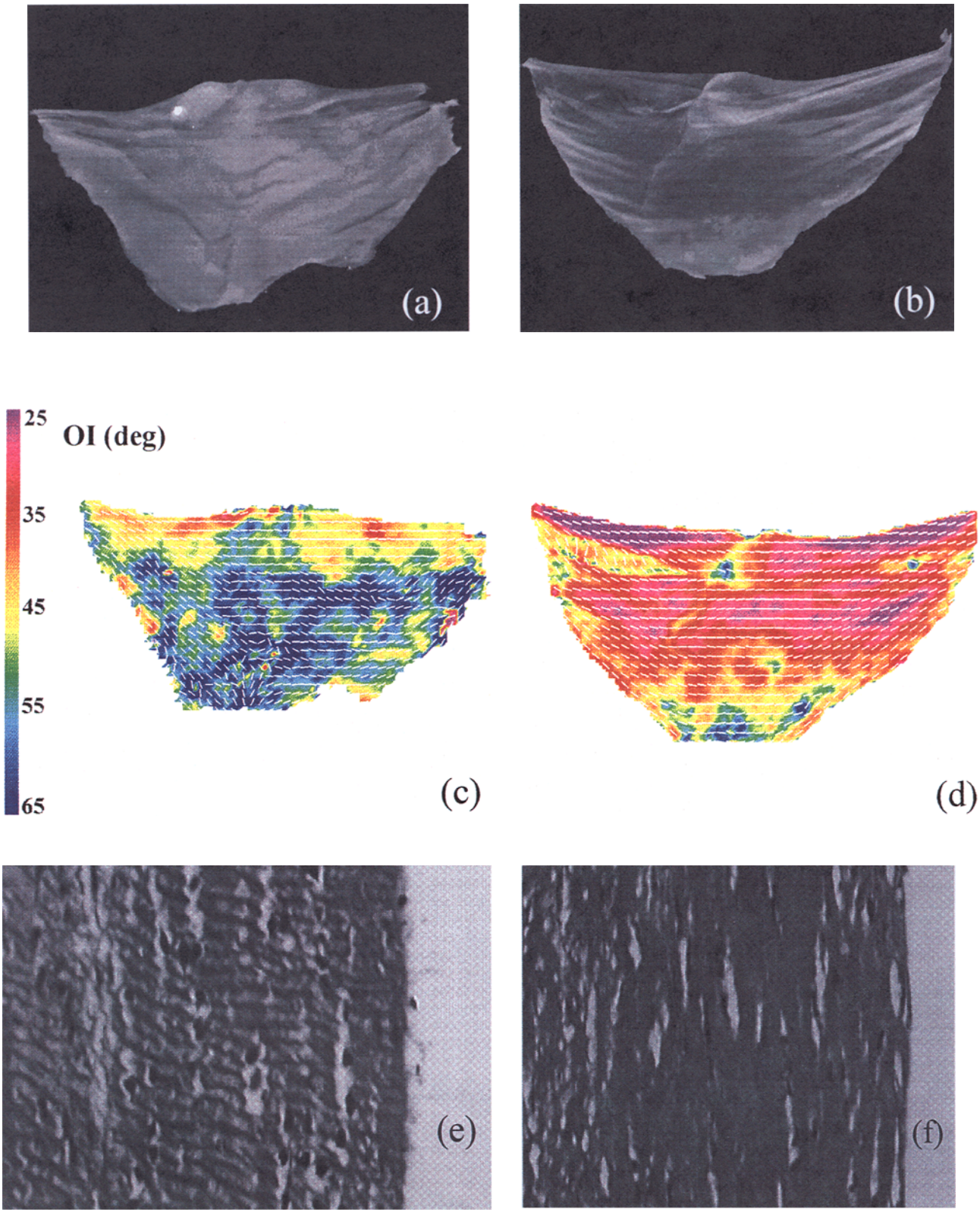

FIGURE 9. Two porcine aortic valve (PAV) leaflets fixed at (a) 0 mm Hg and (b) 4 mm Hg. Each leaflet was SALS tested using a 254-μm-spaced rectilinear grid. The corresponding Φ_c data are shown for each valve as vector plots superposed over color fringe of the OI for (c) 0 mm Hg and (d) 4 mm Hg, with vector data shown for every third test location for clarity. Note the dramatic change in OI with only a 4 mm Hg pressure change, demonstrating substantial mobility of the fiber network at low transvalvular pressures. Histological results for (e) 0 mm Hg and (f) 4 mm Hg showing substantially reduced collagen fiber crimp amplitude, compared with the 0 mm Hg valve. Because the 4 mm Hg valve showed substantially reduced collagen fiber crimp amplitude with little change in preferred directions, the change in OI from 0 to 4 mm Hg is due to a decrease in fiber waviness only.

farther out. Thus, if the fiber diameter distribution was a function of Φ, then the $I(\Phi)$ *versus* Φ data would tend to change with θ. We examined the $I(\Phi)$ *versus* Φ data, normalized to account for the decrease in absolute scattered light intensity for $2° \leq \theta \leq 7°$ to validate this assumption for bovine pericardium and porcine aortic valve leaflets. Both tissue types demonstrated no detectable change in the $I(\Phi)$ intensity distribution for all values of θ, indicating that $I(\Phi)$ is independent of fiber diameter and interfiber spacing for these tissues, *so that the fiber diameter distribution does not affect their fiber orientation measurements.* This result is consistent with the fiber morphology of these tissues, which do not indicate that the collagen bundle diameters are a function of their orientation (8).

Maps of Collagen Fiber Architecture

Fiber-preferred directions can be seen to course smoothly along the circumferential direction in both valves, although the preferred directions are more ordered in the 4 mm Hg leaflet (Fig. 9c, d). However, there was a dramatic change in OI with only a 4 mm Hg pressure change, demonstrating substantial mobility of the fiber network in the PAV at low transvalvular pressures. The nodulii of Aranti can be seen as a more randomly oriented region, and the free edge is clearly delineated in both leaflets as a band of highly oriented fibers along the upper leaflet boundary. Histological examinations indicated that the collagen fiber bundles are closely packed with similar fiber bundle orientations, with the 0 mm Hg showing substantially higher collagen fiber crimp amplitude (Fig. 9e). Because there was little change in the fiber-preferred directions with increased loading (Fig. 9c,d), the improvement in the degree of orientation (lower OI value) was almost entirely due to a decrease in crimp amplitude (Fig. 9e,f). Interestingly, when we fixed bovine pericardium both stress-free and under stress along the fiber-preferred directions (data not shown), changes in OI were found to occur as a result of *both* overall fiber alignment and crimp amplitude.

DISCUSSION

The improved SALS device lends itself to rapid analysis of large areas of tissue without the need for expensive equipment and time-consuming tissue preparations. The device provides high-resolution information on local fiber orientation, to an angular resolution of ~1° and a spatial resolution of ±254 μm. The spatial resolution may at first seem to be rather high, considering the use of a 600 μm $1/e^2$ beam diameter. However, the scanning grid increment (254 μm) represents about one-half a beam diameter, resulting in an overlapping region of only ~33% of the total beam area assuming a circular beam of uniformly distributed light intensity. Furthermore, because the laser has a Gaussian intensity profile, the overlapping area contains in actuality only ~20% of the total light beam intensity. Thus, the spatial resolution of ±254 μm demonstrated in Fig. 7 is made possible from the fact that ~80% of the beam passes through "new" tissue at each succeeding grid location.

Another important aspect of SALS demonstrated in this study is that the distribution of scattered intensity represents the algebraic sum of the contributions from each tissue layer. This was demonstrated by the results for bovine tendon (Figs. 4 and 5) and bovine pericardium (Fig. 8). Thus, SALS measurements represent the total structure of the tissue throughout its thickness, with each layer contributing in proportion of its thickness to the total thickness. Waviness of the collagen fiber bundles will also contribute to the scattered light distribution, but its effects are combined with local fiber orientation and cannot be distinguished. For the aortic leaflet, OI changes occurred only by alterations in waviness, whereas for bovine pericardium OI changes occurred by alterations in both fiber orientation and waviness. This result demonstrates the potential complex changes the fiber architecture of planar tissues undergo with stress and underscores the need for *quantitative* morphological studies.

Polarized light microscopy has often been used to assess the gross collagen fiber architecture of soft tissues by taking advantage of their inherent birefringence (1,15). Hilbert *et al.* (14) applied polarized light microscopy to virgin and accelerated tested bioprosthetic heart valve tissues to visualize fiber directions and crimp. They were able to make accurate crimp measurements and could obtain general information on fiber orientation. However, this technique is difficult to apply as a detailed mapping method, because it requires extensive manual operation, and the inability to distinguish accurately multiple layers of fibers deep within the tissue limits measurement to the more superficial layers. Generally, polarized light microscopy can be a complimentary technique to SALS to provide crimp information, because the same tissues can be used by both techniques without additional processing.

This information obtained by SALS should be useful in many applications, including the study of the microstructure of bioprosthetic heart valves. Bioprosthetic heart valves are generally made from either bovine pericardium or porcine aortic valve tissues, which are chemically treated to stabilize and sterilize them for *in vivo* implantation. *In vivo* valvular degeneration results from collagen fiber disruption leading to leaflet tearing at the free edge, or at points of leaflet attachment to the supporting stent and calcification (3,11,21,32). Thus, quantification of the accumulation of fiber damage by SALS either during *in vitro* accelerated durability testing or investigation of explanted leaflets can potentially improve our understanding of the fatigue process by quantifying regional collagen

fiber damage. We have also recently used SALS to obtain quantitative collagen fiber architecture measurements of tissue-engineered dermal replacements (30) and human cranial dura allografts (24). Thus, SALS lends itself to the study of a wide range of planar soft membranous tissue structures in health and disease.

REFERENCES

1. Baer, E., J. J. Cassidy, and A. Hiltner. Hierarchical structure of collagen and its relationship to the physical properties of tendon. In: Collagen, vol. 2, edited by M. E. Nimni. Boca Raton, FL: CRC Press, 1988, pp. 177–199.
2. Borch, J., P. R. Sundarajan, and R. H. Marchessault. Light scattering by cellulose. III. Morphology of wood. *J. Polym. Sci.* 9:313–329, 1971.
3. Bortolotti, U., A. Milano, and A. Mazzucco. Results of reoperation for primary tissue failure of porcine bioprostheses. *J. Thorac. Cardiovasc. Surg.* 90:564–569, 1985.
4. Chaudhuri, S., H. Nguyen, R. M. Rangayyan, S. Walsh, and C. B. Frank. A Fourier domain directional filtering method for analysis of collagen alignment in ligaments. *IEEE Trans. Biomed. Eng.* BME-34:509–518, 1987.
5. Chien, J. C. W., and E. P. Chang. Small-angle light scattering of reconstituted collagen. *Macromolecules* 5:610–617, 1972.
6. Chuong, C. J., M. S. Sacks, R. L. Johnson, and R. C. Reynolds. On the anisotropy of the diaphragmatic central tendon. *J. Biomech.* 24:563–576, 1991.
7. Cowley, J. M. Principles of image formation. In: Introduction to analytical electron microscopy, chap. 1, edited by J. J. Hren, J. I. Goldstein, and D. C. Joy. New York: Plenum Press, 1979, pp. 1–42.
8. Ferrans, V. J., S. L. Hilbert, T. Tomita, M. Jones, and W. C. Robert. Morphology of collagen in bioprosthetic heart valves. In: Collagen, vol. 3, edited by M. E. Nimni. Boca Raton, FL: CRC Press, 1988, pp. 145–189.
9. Frank, C., B. MacFarlane, P. Edwards, R. Rangayyan, Z. Q. Liu, S. Walsh, and R. Bray. A quantitative analysis of matrix alignment in ligament scars: a comparison of movement versus immobilization in an immature rabbit model. *J. Orthoped. Res.* 9:219–227, 1991.
10. Fung, Y. C. Biomechanics: Mechanical Properties of Living Tissues. New York: Springer Verlag, 1993, pp. 1–568.
11. Gabbay, S., P. Kadam, S. Factor, and T. K. Cheung. Do heart valves bioprostheses degenerate for metabolic or mechanical reasons? *J. Thorac. Cardiovasc. Surg.* 55:208–215, 1988.
12. Guinier, A. X-Ray Diffraction. San Francisco: W. H. Freeman and Company, 1963, pp. 1–378.
13. Halliday, D., and R. Resnick. Physics. New York: John Wiley and Sons, 1960, pp. 1–1214.
14. Hilbert, S. L., V. J. Ferrans, and W. M. Swanson. Optical methods for the nondestructive evaluation of collagen morphology in bioprosthetic heart valves. *J. Biomed. Mater. Res.* 20:1411–1421, 1986.
15. Hukins, D. W. L. Collagen orientation. In: Connective tissue matrix, edited by D. W. L. Hukins. Munich: Verlag, Chemie, 1984, pp. 211–240.
16. Kastelic, J., and E. Baer. Deformation of tendon collagen. In: The mechanical properties of biological materials, edited by J. F. Vincient, and J. D. Currey. Weinheim, U.K.: Society for Experimental Biology Symposium XXXIV, 1980, pp. 397–433.
17. Kronick, P. L., and P. R. Buechler. Fiber orientation in calfskin by laser light scattering or X-ray diffraction and quantitative relation to mechanical properties. *J. Am. Leather Chem. Assoc.* 81:221–229, 1986.
18. Kronick, P. L., M. S. Sacks, and M. Dahms. Vertical fiber defect quantified by small angle light scattering. *Connect. Tiss. Res.* 27:1–13, 1991.
19. Liu, Z. Q., R. M. Rangayyan, and C. B. Frank. Statistical analysis of collagen alignment in ligaments by scale-space analysis. *IEEE Trans. Biomed. Eng.* 38:580–587, 1991.
20. Marshall, G. E. Gaussian laser beam diameters and divergence. In: Optical scanning, edited by G. E. Marshall. New York: Marcel Dekker, 1991, pp. 1–11.
21. Milano, A., U. Bortolotti, and E. Talenti. Calcific degeneration as the main cause of porcine bioprostheses. *Am. J. Cardiol.* 53:1066–1070, 1984.
22. Moritani, M., N. Hayashi, A. Utsuo, and H. Kawai. Light-scattering patterns from collagen films in relation to the texture of a random assembly of anisotropic rods in three dimensions. *Polym. J.* 2:74–87, 1971.
23. Muggli, R., and R. Marton. Light scattering by cellulose. V. Anisotropy scattering by wood fibers. *J. Polym. Sci.* 36:121–139, 1971.
24. Otano, S. E., M. S. Sacks, and T. I. Malinin. Mechanical Behavior of Human Dura Mater, vol. 29. *Proceedings in the 1995 Bioengineering Conference,* Beaver Creek, CO, 1995, pp. 329–330.
25. Purslow, P. P., A. Bigi, A. Ripamonti, and N. Roveri. Collagen fibre reorientation around a crack in biaxially stretched materials. *Int. J. Macromol.* 6:21–25, 1984.
26. Raman, C. V., and M. R. Bhat. The structure and optical behavior of some natural and synthetic fibers. *Proc. Indian Acad. Sci.* A40:109–116, 1954.
27. Sacks, M. S. Focus on materials with scattered light. *Res. Dev.* 30:73–78, 1988.
28. Sacks, M. S., and C. J. Chuong. Characterization of collagen fiber architecture in the canine central tendon. *J. Biomech. Eng.* 114:183–190, 1992.
29. Sacks, M. S., C. J. Chuong, and R. More. Collagen fiber architecture of bovine pericardium. *ASAIO* 40:M632–M637, 1994.
30. Sacks, M. S., M. S. Chuong, W. M. Petroll, M. Kwan, and C. Halberstatd. Collagen fiber architecture of a cultured tissue. *J. Biomech. Eng.* 119:124–127, 1997.
31. Sasaki, N., and S. Odajima. Stress-strain curve and Young's modulus of a collagen molecule as determined by the X-ray diffraction technique. *J. Biomech.* 29:655–658, 1996.
32. Schoen, F. J. Cardiac valve prostheses: review of clinical status and contemporary biomaterial issues. *J. Biomed. Mater. Res.* 21:91–117, 1987.
33. Stein, R. S., P. Erhardt, J. J. van Aartsen, and S. Clough. Theory of light scattering from oriented and fiber structures. *J. Polym. Sci.* 13:1–35, 1966.
34. Stein, R. S., and P. R. Wilson. Scattering of light by polymer films possessing correlated orientation fluctuation. *J. Appl. Phys.* 33:1914–1922, 1962.
35. Whittaker, P., and P. B. Canham. Demonstration of quantitative fabric analysis of tendon collagen using two-dimensional polarized light microscopy. *Matrix* 11:56–62, 1991.

APPENDIX

The Fraunhofer diffraction for a single slit of width w is given by

$$I(\theta) = I_o\left(\frac{\sin \alpha}{\alpha}\right)^2$$

$$\alpha = \frac{\pi w}{\lambda} \sin(\theta), \tag{A1}$$

where I is the scattered light intensity measured along the scattered angle θ, and I_0 is the incident light intensity (13). For two slits separated by a distance d, $I(\theta)$ is now given by

$$I(\theta) = I_o\left(\frac{\sin \alpha}{\alpha}\right)^2 \cos^2(\beta)$$

$$\beta = \frac{\pi d}{\lambda} \sin(\theta), \tag{A2}$$

If the separation of the slits is comparable with the slit width ($w/d \cong 1$), the intensity variations due to slit width and slit separation are approximately equal, where w now represents the average of the slit size and interslit spacing. This is approximately the case for dense connective tissues such as the aortic leaflet. Although possibly limiting the accurate determination fiber diameters from the SALS pattern, all orientation information is preserved because the fibers and the spaces between the fiber have the same orientation.